Energy Proceedings
Vol 65, 2026
ISSN 2004-2965

Effect of Water Saturation on Oil Recovery and CO_2 Storage during Hot Flue gas flooding

Yuan Yuan[1*], Renbao Zhao[1*], Guangsen Zhu[1], Jiaying Wang[1], Bin Liu[1]

1 State Key Laboratory of Petroleum Resources and Engineering, China University of Petroleum, Beijing 102249, China.

(Corresponding Author: yuany9939@163.com, zhaorenbao@vip.sina.com)

ABSTRACT

Carbon dioxide capture, utilization, and storage (CCUS) technology is a key pathway for achieving sustainable low-carbon utilization of fossil energy. Currently, the coupled development of CCUS and enhanced oil recovery (EOR) has made preliminary progress and is moving towards large-scale engineering applications. To balance resource maximization and carbon reduction goals, this paper investigates the impact of different water saturations (0%, 40%, 60%) on thermal propagation, recovery rate, and CO_2 storage behavior by preheating the flue gas to 300 °C before injecting it into a sandpack tube (ST). The results indicate that at a water saturation of 40%, the average temperature change rate, standard deviation, and coefficient of variation are minimized, suggesting that the synergistic effect of steam and flue gas effectively enhances heat transfer efficiency and extends the advance distance of the thermal front. Under this condition, the ultimate oil recovery and CO_2 storage are improved to 72.2% and 17.7%, respectively, significantly better than the cases of no water and high water content. Moderate water content promotes oil recovery efficiency and carbon storage capacity through a synergistic mechanism involving viscosity reduction, improved steam convective heat transfer, and gas swelling. This study clarifies the optimal range of water content in the thermal flue gas flooding (FGF) process and provides support for field flue gas reinjection and in-situ storage.

Keywords: FGF, Water saturation, Storage, CCUS, EOR

NONMENCLATURE

Abbreviations	
CCUS	Carbon dioxide capture, utilization, and storage technology
EOR	Enhanced oil recovery
FGF	Flue gas flooding
ISC	In-situ combustion
ST	Sandpack tube
PV	Pore volume
Sw	Water saturation

1. INTRODUCTION

CCUS is regarded as a crucial pathway to achieving near-zero emissions from fossil energy sources, playing an important role in the global framework for greenhouse gas reduction [1]. In heavy oil development, thermal recovery processes such as in-situ combustion or steam flooding are widely applied, and the process typically generates flue gas containing about 9-15% CO_2 together with abundant N_2 [2]. These gases serve as both sources of greenhouse gas emissions and potential economical injection mediums for EOR [3]. However, most flue gas is currently released directly into the atmosphere, wasting valuable gas resources and increasing the carbon emission burden [4]. If flue gas is captured and reinjected underground, it can expand the thermal influence range through the effects of CO_2 swelling and viscosity reduction, nitrogen energy support, and steam heat transfer, thereby achieving the dual objectives of in-situ CO_2 storage and enhanced heavy oil production [5].

The long-term stability of geological sequestration depends on four capture mechanisms: structure, residue, solubility and minerals [6]. The injection of unseparated flue gas in the oil reservoir can simultaneously undergo four types of processes: structural trapping, gas-phase residue, dissolution into formation fluids, and adsorption onto organic matter. Theoretically, it has a storage potential comparable to that of pure CO_2. However, the high proportion of N2 in flue gas and the complex impurities of O_2 and water vapor lead to an increase in the minimum mixed-phase pressure, a higher risk of corrosion and scaling, and more complex heat transfer and seepage behaviors [7]. There is an urgent need to carry out targeted experiments and model studies.

This is a paper for the 17th International Conference on Applied Energy (ICAE2025), December 8-12, 2025, Bangkok, Thailand.

At present, most of the public literature on flue gas flooding and storage is based on numerical simulation. Physical experiments, especially studies under high-temperature conditions, are relatively scarce. There is a lack of quantitative assessment of the coupling mechanism between water saturation and temperature field evolution. In this study, a physical simulation device for heated flue gas was constructed, and the effects of different initial water saturations on heat transfer distance, oil recovery, and CO_2 storage behavior were investigated. The innovation of this study lies in systematically quantifying at the physical experimental scale the influence of water saturation on the coupling effect of heated flue gas oil displacement and storage, improving the understanding of the mechanism of flue gas injection.

2. MATERIAL AND METHODS

2.1 Material

The oil used in the experiment was collected from the JD oilfield, China. Dehydration was performed using an electric dehydration apparatus (DEG-4C) before the experiment. The density of the sufficiently dehydrated oil is 0.80 g/cm³ at ambient conditions, and the variation of oil viscosity with temperature is presented in Fig. 1. The oil viscosity is 19.2 mPa·s (at a shear rate of 10 s^{-1}) at 50°C. The sand samples used in the experiment are quartz sand with different mesh ranges (60-80 and 80-100). Additionally, a K-type thermocouple (produced by OMEGA) was used to monitor the temperature changes in the ST.

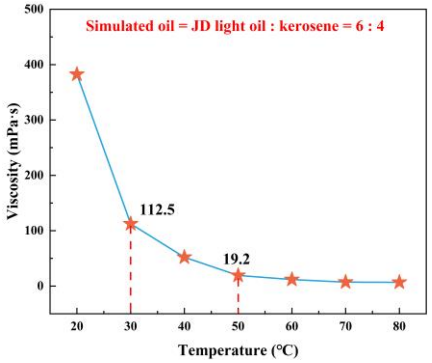

Fig. 1 The viscosity of heavy oil changes at different temperatures

2.2 Experimental procedures

The schematic diagram of the ST experiment is shown in Fig. 2. The ST device mainly includes a gas injection system, a temperature control device, a ST, a data monitoring and acquisition system, and an online gas analyzer (China Wuhan Cubic Optoelectronics Co., LTD.). The ST themselves are made of titanium alloy, with lengths of 60 and 70 cm respectively and inner diameters of 3.8 cm each. The ST (70cm) is filled with 80-100 mesh quartz sand and wrapped with tracing belt to heat the flue gas. Oil sand is filled in the 60cm ST. Both ST are wrapped with quartz wool on the outside to reduce heat loss. Five temperature detection points (named as thermal well) are distributed along ST, marked as T2, T3, T4, T5, and T6, which are 6 cm, 18 cm, 30 cm, 42 cm, and 54 cm away from the gas injection well, respectively. Both ends of ST are sealed with flanges and graphite ferrules. The production well is connected to the gas-liquid separator, and part of the separated gas is detected and analyzed by an online gas analyzer.

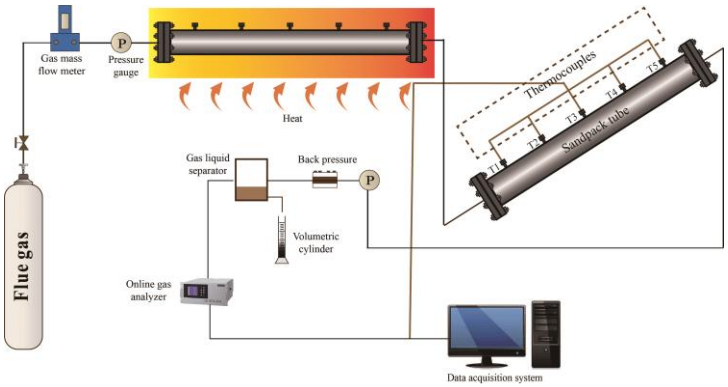

Fig. 2 The schematic diagram of kinetic cell and combustion tube experiments

The physical parameters of the ST are shown in Table 1. The experimental steps are as follows: Oil sand was uniformly packed into the ST, weighed, and sealed within the apparatus. After confirming gas tightness with N2 injection, flue gas was introduced to saturate the first ST, and the system was preheated using a heating program and tracing belt. Continuous flue gas injection was then initiated, while the airflow rate, injection pressure, and back pressure were adjusted to preset values and kept stable. Throughout the experiment, temperatures at

monitoring wells and the volumetric fractions of produced gases were recorded in real time, and liquid samples were collected every 10 min. The experiment was terminated once the liquid production rate declined sharply and only little amounts of liquid were recovered.

Table 1. Experimental scheme for FGF

No.	Composition of flue gas	Permeability (um2)	Water saturetion （%）
Ⅰ	10%CO2+90%N2	51.2	0
Ⅱ	10%CO2+90%N2	52.1	40
Ⅲ	10%CO2+90%N2	49.1	60

3. RESULTS AND DISCUSSION

3.1 Characteristics of temperature field

During the experiment, the temperatures at each thermal well continued to rise with the injection of PV. The temperature profile is shown in Fig. 3. Under conditions of no water and 40% Sw, the final temperatures from T2 to T6 all exceed 200℃, and the heat can continuously spread downstream. When the Sw is 60%, the final temperatures of T5 and T6 are only 160℃ and 148℃ respectively, with significant temperature attenuation. This indicates that excessive Sw will inhibit the temperature expansion along the range.

To further quantify heating uniformity, the average temperature change rate r of each section was used as the basic indicator, and statistical parameters including the mean, standard deviation (s), coefficient of variation (CV), and range (Δr) of r were calculated. The results show that the Δr of the 40% Sw is only 0.00720 ℃·s⁻¹, which is the smallest among the three experiments. The s is only 0.0027, the CV is 18.16%, the heating rate from T2 to T6 is close, the thermal front advancement is relatively stable, the gas influence range is larger, and the heat transfer efficiency is higher. Under waterless conditions, the highest (0.0242℃·s⁻¹), Δr increases to 0.01037 ℃·s⁻¹, the phenomenon of uneven temperature rise is prominent, and the gas channels are more likely to occur, resulting in an uneven distribution of heat. When the Sw was 60%, it was close to that when the Sw was 40% (0.0168 and 0.0149℃·s⁻¹), but s and CV increased to 0.0036℃·s⁻¹ and 21.94% respectively, Δr reached 0.0092 ℃·s⁻¹, and the terminal temperature was significantly lower. This indicates that although convective heat transfer exists, excessive water strongly absorbs heat and increases the heat capacity of system. At the same time, it reduces the relative permeability and effective mobility of the gas phase, hindering full contact of hot flue gas with the cold oil and weakening heat transfer in the middle and later stages.

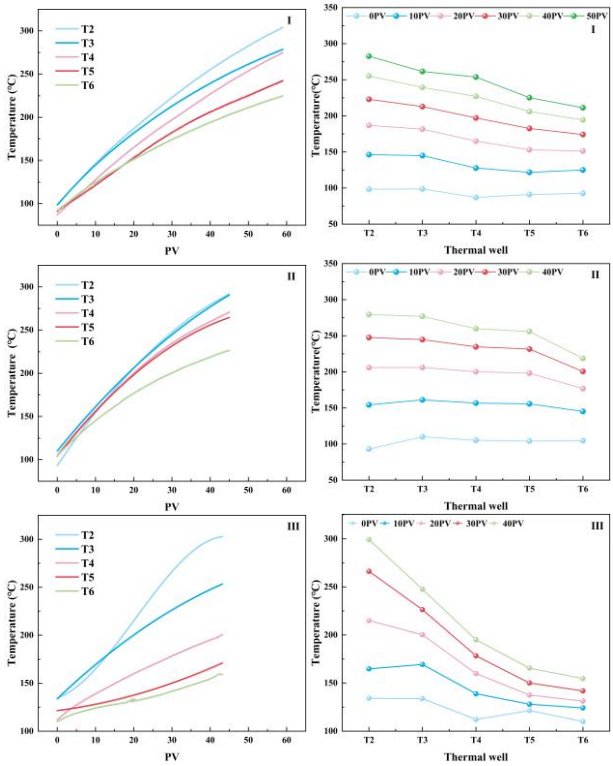

Fig. 3. The temperatures change over time

Table 2. Temperature change rate along the tube

No.	T2-T3	T3-T4	T4-T5	T5-T6	T3-T6
Ⅰ	0.02907	0.02541	0.02655	0.02136	0.0187
Ⅱ	0.01794	0.01642	0.01473	0.01443	0.01074
Ⅲ	0.02246	0.01673	0.01594	0.01408	0.01324

$$\bar{r} = \frac{1}{n}\sum_{i=1}^{n} r_i \quad (1)$$

$$s = \sqrt{\frac{1}{n-1}\sum_{i=1}^{n}\left(r_i - \bar{r}\right)^2} \quad (2)$$

$$CV = \frac{s}{\bar{r}} \quad (3)$$

$$\Delta r = \max(r_i) - \min(r_i) \quad (4)$$

Table 3. Comparison of the statistical index of the average temperature change rate

No.	$\bar{r}$ （℃/s）	s （℃/s）	CV (%)	Δr （℃/s）
Ⅰ	0.0242	0.0042	17.15	0.0104
Ⅱ	0.0149	0.0027	18.16	0.0072
Ⅲ	0.0165	0.0036	21.94	0.0092

3.2 Variation of effluent gases compositions

The compositions variation of effluent gases with time is shown in Fig. 4. In ST with quartz sand, crude oil and kaolin, the migration and distribution of CO_2 mainly include three paths. (i) escape with the gas flow to the

outlet, (ii) dissolution in the crude oil or aqueous phase within the pores, and (iii) retention on the surface of solids such as kaolin via physical adsorption. Since quartz sand has almost no adsorption capacity for CO_2, the effective retention of CO_2 in the system mainly depends on the surface adsorption effect of kaolin and its solubility in the fluid. However, the adsorption capacity of kaolin is usually only at the milligram level, and its contribution is extremely limited. Meanwhile, the dissolution behavior of CO_2 by crude oil is significantly affected by temperature and pressure. Reducing pressure or increasing temperature will both cause the gas to escape again. In addition, the system lacks carbonate or feldspar minerals, and the mineral fixation reaction is not obvious, thereby restricting the establishment of a long-term storage mechanism. The experimental results show that the storage efficiency of CO_2 is closely related to the Sw conditions. Under different PV (1 PV, 2 PV, 5 PV and ultimate ventilation volume), the sequestration rates of CO_2 (SCO_2) under anhydrous conditions were 18.8%, 18.4%, 17.7% and 16.5% respectively. When the Sw is 40%, it is always the highest, which are 19.3%, 18.9%, 18.5% and 17.7% respectively. When the Sw is 60%, it drops to 17.4%, 17.3%, 17.0%, and 15.6% respectively. Comprehensive analysis shows that although some CO_2 remains at the oil phase, gas phase or solid phase interface in the ST, these mechanisms are essentially difficult to achieve long-term stable storage. Under the current system and experimental conditions, the maximum storage rate of CO_2 does not exceed 20%, mainly limited by the capacity and stability of the two mechanisms of physical adsorption and dissolution.

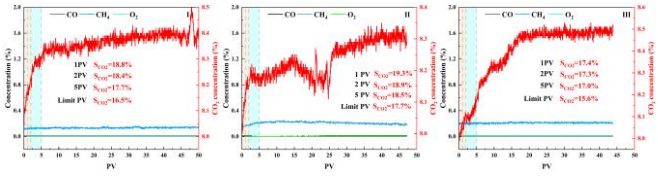

Fig. 4 The compositions variation of effluent gases with time

3.3 Verification of Chemical Ignition in 3D Model

The variation of the oil recovery is shown in Fig. 5. When the Sw was 0%, the oil recovery was only 11.2% when about 5 PV was injected, the slope was the maximum within 15 to 30PV, and the curve tended to plateau around 60PV. The final limit oil recovery was 67.4%. When the Sw increases to 40%, the oil recovery increases. Some pores are filled with water, which can change gas distribution. The CO2 swelling effect and N2 displacement work in synergy within a larger contact area. The oil recovery can reach 18.5% at 5 PV, and it is approaching the plateau at about 30 PV. The limit oil recovery rose to 72.2%, an increase of approximately 5% compared to when there was no water. When the Sw reaches 60%, the rate of increase in oil recovery slows down. The gas needs to overcome greater resistance from the aqueous phase to come into contact with the oil. The highly soluble CO_2 is partially absorbed by the aqueous phase, reducing its contribution to the viscosity of crude oil and gas swelling. The oil recovery around 5 PV is approximately 12.3%, and the growth rate remains relatively linear in the range of 10 to 30PV. After 45 PV, the oil recovery slowed down, and the final oil recovery remained at 61.2%, significantly lower than the previous two cases.

Overall, water saturation has a comprehensive regulatory effect on heat transfer and the characteristics of gas-liquid two-phase seepage. An appropriate amount of water can not only act as a heat buffer medium during the displacement process, absorbing and releasing sensible heat again, but also form steam in the high-temperature zone to promote convective heat transfer and reduce viscosity, while increasing the heated volume of the oil phase and inhibiting the premature gas escape of N2. Therefore, when the Sw is 40%, it not only accelerates early displacement but also maintains a relatively uniform temperature propagation, thereby achieving the highest ultimate oil recovery. Local overheating is prone to generating solid particles and reducing pore connectivity under there is no water condition. Although the oil recovery can still be continuously improved by gas-phase displacement in the middle and later stages, the overall efficiency is still lower than that of Sw is 40%. When the Sw rises to 60%, the excess water consumes a large amount of heat during the phase change process, causing the temperature to drop. And then, the carbon dioxide swelling effect is inhibited. At the same time, the high Sw reduces the relative permeability of the oil phase and promotes the early occurrence of steam channel and water penetration phenomena, resulting in a rapid slowdown of the harvest curve in the middle and later stages and its termination at a relatively low level.

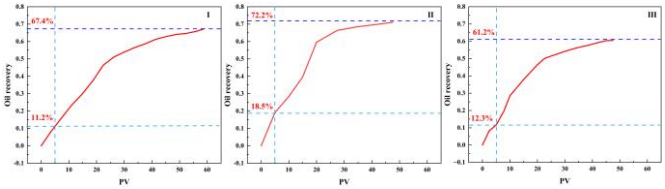

Fig. 5 The recovery rate of the experiment

The oil recovery process of hot FGF can be divided into three stages, referred to as the rapid oil production period, the high efficiency stable production period, and the production decline period, as shown in Fig. 6. Rapid oil production period (I): corresponding to 0 to approximately 10 PV. High-temperature flue gas is rapidly conducted to the area near the injection well area, significantly reducing the viscosity of crude oil. At the same time, a large amount of CO_2 dissolves in the crude oil, forming small and uniform foam, which significantly reduces displacement resistance. At this stage, the produced liquid is light brown foamy oil with uniform gas-liquid distribution. The oil recovery increases rapidly within an extremely small PV, and approximately 30% to 50% of the limit oil recovery can be utilized. High efficiency and stable production period (II): corresponding to approximately 10 PV to 40 PV. The oil in ST has exchanged heat fully with the injected gas. The viscosity of the crude oil continues to decrease but at a slower rate. Under high-temperature conditions, some light components evaporate and work in synergy with CO_2 to enhance the fluidity of the crude oil. The produced liquid turns into a homogeneous emulsion with a darker color. At this stage, the slope of the oil recovery curve relatively decreases but remains stable, the utilization efficiency is high, and the oil recovery steadily approaches the limit level. Production decline period (III): After 40 PV. After the light and medium components are extensively utilized, the residual oil is mainly composed of heavy components, and the extraction and swelling effects significantly decline. The gas is preferentially produced through high-permeability channels, exacerbating sweep heterogeneity. The produced liquid is characterized by dark heavy oil mixed with a small number of large bubbles, with the curve tending towards a plateau and the contribution of oil increase per unit PV being extremely low. Overall, hot flue gas flooding, relying on the dual mechanisms of high-temperature viscosity reduction and carbon dioxide swelling, achieved efficient utilization in the early stage.

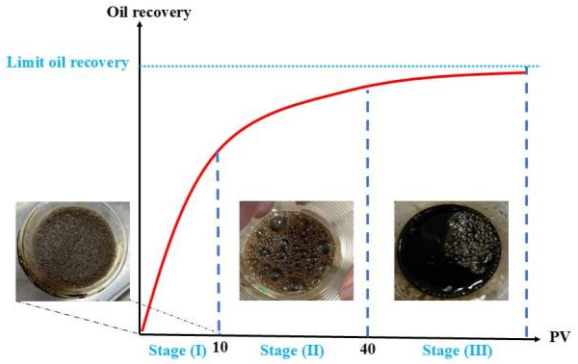

Fig. 6 Stage division of hot flue gas flooding

Fig. 7 shows the appearance of the oil sand distribution after gas displacement in the hot flue gas. In the absence of water, the color gradually changes from light gray at the top to dark brown at the bottom with a pore-like mass notably forming at the lower end. This observation indicates that when high-temperature gas directly contacts crude oil, the lighter components evaporate rapidly, while the heavier components undergo thermal condensation due to localized overheating, resulting in a strong and non-uniform block. When the *Sw* is 40%, the overall profile appears light gray, characterized by significantly reduced and uniformly distributed clumps. The volume of the water and sand mixing zone at the bottom marked by the red box is limited, indicating that the steam generation and condensation cycle occurs here, which not only balances the temperature gradient but also reduces the viscosity of the oil phase, achieving the best displacement homogeneity. When the *Sw* is 60%, a large area of light brown unused zone appears. The upper part only has scattered lumps, while the lower part is blocked by a larger water and sand mixture zone. The excess water phase absorbs sensible heat and occupies the pores, resulting in insufficient temperature rise of the oil phase, inhibition of CO_2 swelling and evaporation displacement effects, and the residual oil is distributed sparsely.

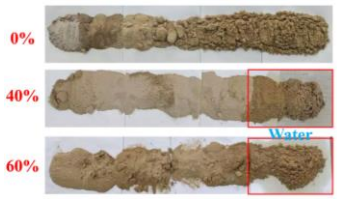

Fig. 7. Stage division of hot FGF

4. DISCUSSION

Hot FGF primarily enhances crude oil utilization through the synergistic effects of gas displacement and thermal mechanisms, as illustrated in Fig. 8. Flue gas injection serves to replenish formation pressure and facilitate the flow of crude oil towards the production endpoint. The principal component, CO_2, when dissolved in crude oil, markedly reduces viscosity, induces volume expansion, improves fluidity ratios, and enhances sweep efficiency. Another significant component, N_2, although insoluble in oil, can create drainage channels through gravitational effects, while also diluting the saturation of the oil phase and increasing the relative permeability of crude oil. Furthermore, high-temperature flue gas exerts notable thermal effects, further reducing the viscosity of

crude oil and causing thermal expansion between crude oil and formation water. Under conditions of high temperature and pressure, CO_2 is capable of extracting lighter components, potentially forming a mixed-phase or near-mixed-phase system, significantly reducing interfacial tension and improving the efficiency of micro-oil displacement. Water plays a crucial role in regulating the displacement mechanism of hot FGF. Under high-temperature conditions, the injected water undergoes a phase change into water vapor, which releases latent heat that significantly exceeds gas conduction. This process has a deeper and more uniform influence on the thermal effect of porous media, and improves the solubility of CO2 in crude oil. The steam and hot water also improve the mobility ratio, suppresses early breakthrough, and increases sweep efficiency. Laterally expanding steam cavities help prevent N_2 overcoating, while condensate water sinks to create a blocking effect that stabilizes the advance of the thermal front. Water saturation governs the extent of these mechanisms. At moderate Sw (e.g., 40%), formation water and injected hot fluid enhancing convective heat transfer, delaying leading-edge cooling, and improving multiphase displacement efficiency. Insufficient water leads to local overheating, while excessive water results in heat absorption and increased flow resistance, ultimately reducing displacement efficiency and CO_2 retention.

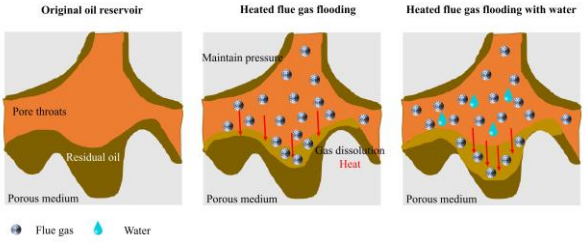

Fig. 8. Diagram of the mechanism of hot FGF

5. CONCLUSIONS

In this study, hot FGF experiments were conducted under different water saturation (0%, 40%, and 60%). The mechanisms and synergistic effects on oil recovery and CO_2 storage efficiency were quantitatively evaluated, and the following conclusions were drawn:

(1) Water saturation is a key variable governing the coupled effects of heat transfer, fluid flow, and reaction. Under experimental conditions, when the Sw is 40%, the distribution of temperature change rate is the most uniform (minimum Δr is 0.0072 °C/s), the heat transfer distance is the longest, and the advancement of the thermal front is the most stable.

(2) Both oil recovery and CO_2 storage exhibit an optimal Sw. At Sw = 40%, recovery and storage reach maxima of 72.2% and 17.7%, respectively. This optimum results from steam-enhanced convection, balanced gas–liquid flow, and improved CO_2 reaction pathways, whereas too little or too much water suppresses heat transfer and CO_2 storage.

ACKNOWLEDGEMENT

This work was supported by the Joint Fund Program of The National Natural Science Foundation of China (Grant No. 52274052).

REFERENCE

[1Wang Z, Li S, Li Z. A novel strategy to reduce carbon emissions of heavy oil thermal recovery: Condensation heat transfer performance of flue gas-assisted steam flooding. Applied Thermal Engineering 2022;205:118076.

[2] Wu Z, Liu H, Wang X. 3D Experimental Investigation on Enhanced Oil Recovery by Flue Gas Coupled with Steam in Thick Oil Reservoirs. Energy & Fuels 2018;32(1):279-86.

[3] Li S, Li Z, Sun X. Effect of flue gas and n -hexane on heavy oil properties in steam flooding process. Fuel 2017;187:84-93.

[4] Pang Z, Qi P, Zhang F, Ge T, Liu H. The Experimental Analysis of the Role of Flue Gas Injection for Horizontal Well Steam Flooding. Journal of Energy Resources Technology 2018;140(10).

[5] Santibanez-Borda E, Govindan R, Elahi N, Korre A, Durucan S. Maximising the Dynamic CO2 storage Capacity through the Optimisation of CO2 Injection and Brine Production Rates. International Journal of Greenhouse Gas Control 2019;80:76-95.

[6] Wang Z, Li Z, López-Ochoa LM. Roles of Flue Gas in Promoting Steam Flow and Heat Transfer in Multithermal Fluid Flooding. Mathematical Problems in Engineering 2019;2019(1).

[7] Han H, Li S, Ma D, Ji Z, Yu H, Chen X. Investigation of flue gas displacement and storage after the water flooding in a full diameter conglomerate long-core. Petroleum Exploration and Development 2018;45(5):903-9.